Annual Conference Flow2017 for Microfluidic, 3-5 July, Paris-France

Numerical study on the static response of coated microbubbles

Alkmini D. Lytra & Nikos A. Pelekasis
Lab. of Fluid Mechanics & Turbomachinery, Dep. of Mechanical Engineering, University of Thessaly, Greece
pel@uth.gr, http://contrast-aristeia.mie.uth.gr/

Scope & Abstract

The present poster presents two theoretical models of the static response of coated microbubbles, (MB), also known as contrast agents. In the first model the MB is subject to a distributed load in order to describe the response under the atomic force microscope (AFM), while in the second the MB is subject to a uniform static load.

In both models , two types of MB are considered, those which are coated with polymer and those with lipid monolayer. The equilibrium equations are solved in axisymmetric form via FEM and two dimensionless numbers emerge: the dimensionless bending and dimensionless pressure. We use the B-cubic splines as basis functions and we perform simple or arc-length continuation.

In the contact problem, a long range attractive-short range repulsive potential describes the thinning of the intervening liquid film as the cantilever approaches the shell. We compare the numerical results with available AFM data and we propose a novel method via asymptotic analysis for the estimation of elastic properties from the force-deformation curve.

In the uniform pressure model appropriate stability calculations reveal a rich bifurcation diagram, corresponding to non-spherical shapes, which is in agreement with dynamic calculations when static equilibrium is reached.

In both cases, parametric study in the space of dimensionless numbers is performed.

Theoretical Modelling

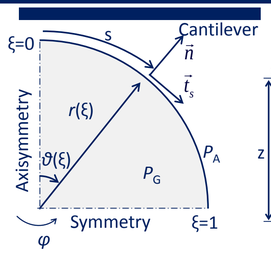

Reference State

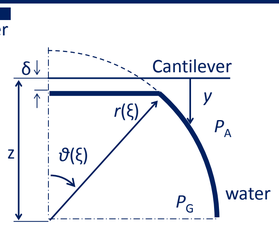

Intermolecular forces – contact model

Equilibrium equations[1–2]:

Balance of stresses: $\Delta P \underline{\underline{I}} \cdot \vec{n} = 2k_m(\gamma_{BW} + W)\vec{n} - \vec{\nabla}_s \cdot \underline{\underline{T}} + \frac{\partial W}{\partial n}\vec{n}$

Isothermal Gas Compression: $P_G V_f^{\gamma} = P_A V_i^{\gamma} \quad \Delta P \equiv P_G - P_A$

Adhesive potential[3]:

$$W(y) = W_0\left[\left(\frac{\delta_A}{y}\right)^4 - 4\left(\frac{\delta_A}{y}\right)^2\right], \delta_A = 50\ nm, W_0 = 10^{-4}\ N/m$$

Boundary conditions:

$$r_{\xi}(\xi = 0\ \&\ 1) = 0,\ \theta_{\xi\xi}(\xi = 0\ \&\ 1) = 0$$

and $\theta(\xi = 0) = 0,\ \theta(\xi = 1) = \frac{\pi}{2}$

Dimensionless parameters:

$$\hat{k}_b = \frac{k_b}{\chi R_o^2};\ \hat{P}_A = \frac{P_A R_o}{\chi};\ \hat{\gamma}_{BW} = \frac{\gamma_{BW}}{\chi};\ \hat{W} = \frac{W}{\chi};\ \hat{\chi} = 1.$$

Total force on the shell due to intemolecular forces:

$$\vec{F} = -\int_A \left(\frac{\partial W}{\partial n} + 2k_m W\right) dA\vec{e}_z$$

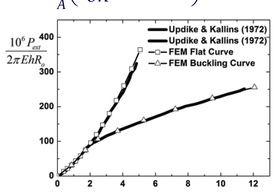

Fig.1 Comparison against the Updike & Kalnins[4] solution

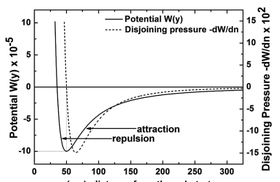

Fig.2 Distribution of the adhesive potential & the disjoining pressure along the distance from the substrate

Results

MB under a rigid & flat surface–Elastic properties characterization–Comparison against AFM data

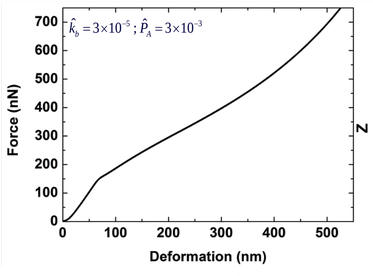

Fig.3 Force-deformation curve

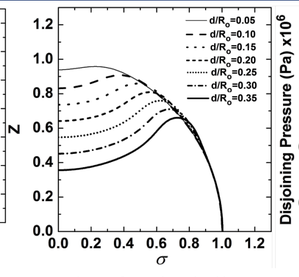

Fig.4 Deformed MB-buckling

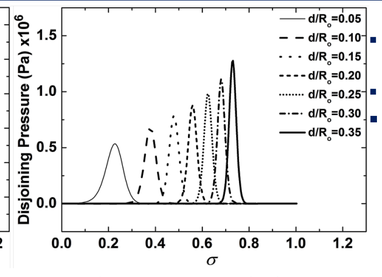

Fig.5 Disjoining pressure distribution

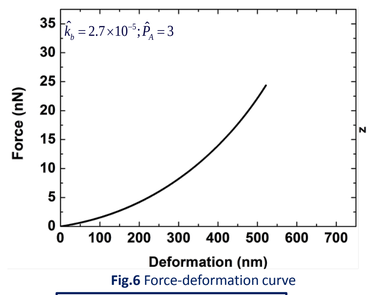

Fig.6 Force-deformation curve

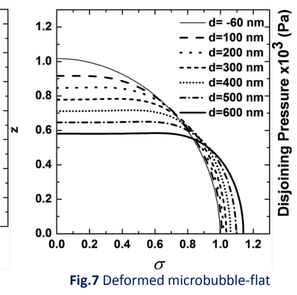

Fig.7 Deformed microbubble-flat

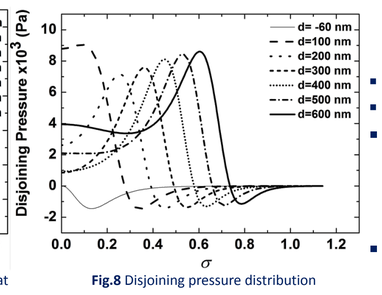

Fig.8 Disjoining pressure distribution

Polymers

Reissner for linear response[5]:

$$F = 8\sqrt{\chi k_b}\frac{\Delta}{R_o}$$

Pogorelov for buckling[5]:

$$F = \left[\frac{3.56E^2h^5}{\left(1-\nu^2\right)^2 R_o^2}\Delta\right]^{0.5}$$

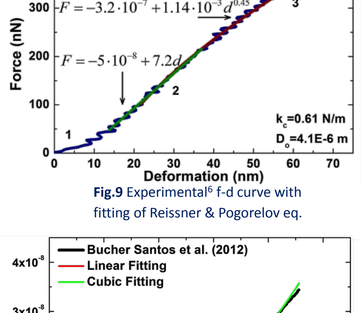

Fig.9 Experimental[6] f-d curve with fitting of Reissner & Pogorelov eq.

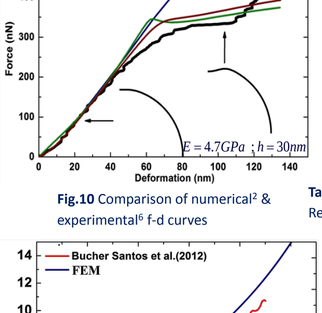

Fig.10 Comparison of numerical[2] & experimental[6] f-d curves

Lipids

Reissner for linear response[5]:

$$F = 8\sqrt{\chi k_b}\frac{\Delta}{R_o}$$

Response dominated by gas compression[2 & 8]:

$$F = \frac{4\pi\chi}{R_o^2}\Delta^3$$

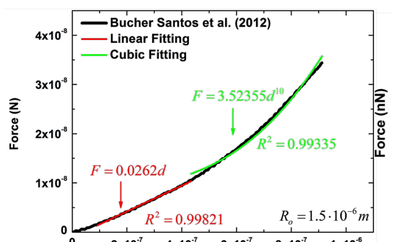

Fig.11 Experimental[9] f-d curve with fitting of Reissner & Pogorelov eq.

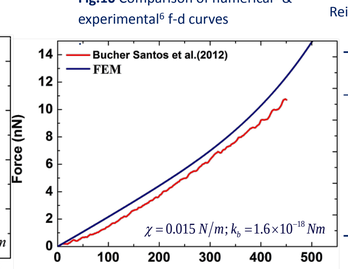

Fig.12 Comparison of numerical[2] & experimental[9] f-d curves

Simulation: MB covered with polymer

- E=2.1 GPa, h=25 nm (χ=51 N/m; k_b=3.4·10^{-15} Nm)-Hook
- Ro=1.5 μm; ν=0.5
- The response in this case follows the classical initial linear regime (~Δ-Reissner type) and then buckling takes place, characterized by non-linear response (~$\Delta^{0.5}$-Pogorelov regime). For relative high values of deformation a non-linear regime is detected (~Δ^3) dominated by the gas pressure.

Simulation: MB covered with lipid

- χ=5·10^{-2}N/m ; k_b=3·10^{-18} Nm-Mooney-Rivlin
- Ro=1.5 μm; ν=0.5
- Initially, the response is linear, but then buckling is bypassed to a non-linear regime (~Δ^3), where gas pressure dominates.
- In both case the pick of the disjoining pressure is located at the end of the contact line.

	Experimental Values[6]		Asymptotic Estimation[7]	
D_o [μm]	E [GPa]	h [nm]	E [GPa]	h [nm]
2.6	10-16	20	8.5	25
4.1	2.5-6	31	6.1	31
3.1	6-10	23	3.4	35
4.0	2.5-6	30	4.7	30
5.5	1-3	41	1.7	47

Table 1 Comparison of the experimental and calculated via the Reissner-Pogorelov eq. values of Young modulus and shell thickness.

	Experimental Values[9]		Asymptotic Estimation[2 & 8]	
D_o [μm]	χ [N/m]	k_b [Nm]	χ [N/m]	k_b [Nm]
2.06	0.050	1.38·10^{-19}	0.005	1.23·10^{-15}
2.94	0.075	2.08·10^{-19}	0.011	1.77·10^{-15}
3.50	0.075	2.08·10^{-19}	0.011	2.32·10^{-15}
4.22	0.150	4.17·10^{-19}	0.016	1.86·10^{-15}

Table 2 Comparison of the experimental and calculated via the Reissner-Gas dominated eq. values of area dilatation and bending stiffness.

MB subject to a uniform & static pressure field - Bifurcation diagrams

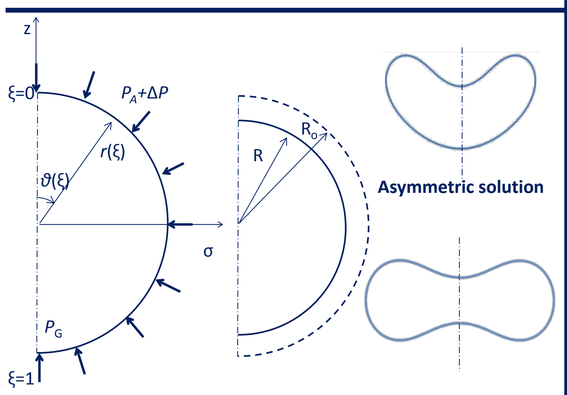

Reference state **Spherical solution** **Symmetric solution**

Equilibrium equations[1, 2, 10]:

Balance of stresses: $(P_G - P_A - \Delta P)\underline{\underline{I}} \cdot \vec{n} = 2k_m\gamma_{BW}\vec{n} - \vec{\nabla}_s \cdot \underline{\underline{T}}$

Isothermal Gas Compression: $P_G V_f^{\gamma} = P_A V_i^{\gamma}$

$\varepsilon = \Delta P / P_A\ ;\ \tilde{V} = V/V_i$

Imposition of the mass center at the axis origin:

$$z_{CM} = \frac{\int_V \vec{r}\cdot\vec{e}_z dV}{V} = 0$$

Boundary conditions:

$$r_{\xi}(\xi = 0\ \&\ 1) = 0,\ \theta_{\xi\xi}(\xi = 0\ \&\ 1) = 0$$

and $\theta(\xi = 0) = 0,\ \theta(\xi = 1) = \pi$

with:

$$\vec{q} = \vec{\nabla}_s \cdot \underline{\underline{m}} \cdot \left(\underline{\underline{I}} - \vec{n}\vec{n}\right), \sigma = r\sin\theta$$

$$\underline{\underline{m}} = m_{ss}\vec{t}_s\vec{t}_s + m_{\varphi\varphi}\vec{t}_\varphi\vec{t}_\varphi\ ;\ \underline{\underline{T}} = \tau_{ss}\vec{t}_s\vec{t}_s + \tau_{\varphi\varphi}\vec{t}_\varphi\vec{t}_\varphi + q\vec{t}_s\vec{n}$$

$$\underline{\underline{\tau}} = \frac{2}{J_s}\left[\frac{\partial w}{\partial I_1}\underline{\underline{A}}\cdot\underline{\underline{A}}^T + \frac{\partial w}{\partial I_2}J_s^2\left(\underline{\underline{I}} - \vec{n}\vec{n}\right)\right]$$

w: Elastic energy functions (Hook, Mooney-Rivlin)[11]

$$m_{ii} = \frac{k_b}{\lambda_j}\left(K_i + \nu K_j\right),\ i, j \to s, \varphi\ \text{direction},$$

I_1, I_2 Invariants of Green-Lagrange deformation tensor

$$G_s = \frac{\chi}{2(1+\nu)}, G_{MR} = \frac{\chi}{3}, \chi = Eh, k_b = \frac{Eh^3}{12(1-\nu^2)}$$

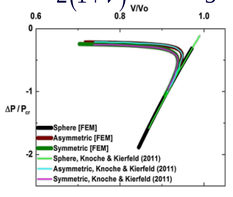

Fig.11 Comparison against the Knoche & Kierfeld solution[12]

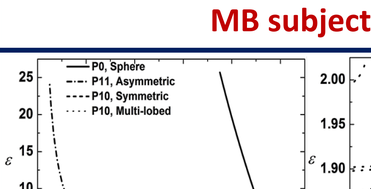

Fig.13 Bifurcation diagram

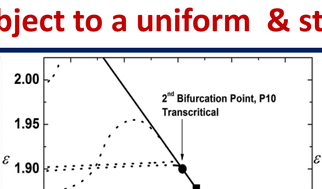

Fig.14 Zoom in the bifurcation points

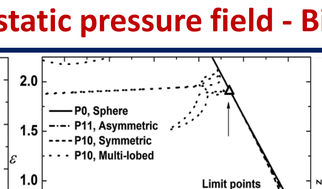

Fig.15 Zoom in the limit points

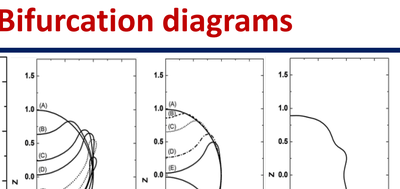

Fig.16 Asymmetric, symmetric & multi-lobed solutions

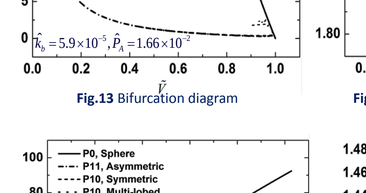

Fig.17 Energy diagram

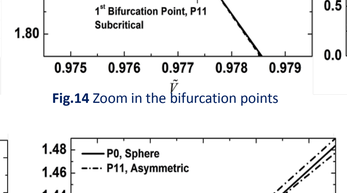

Fig.18 Energy diagram, comparison of spherical & asymmetric solutions

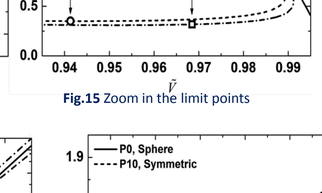

Fig.19 Energy diagram, comparison of spherical & symmetric solutions

Simulation: MB covered with polymer

- h=23.1 nm, G_s= 88 MPa
- R_o=1 μm, ν=0.5, Hook, γ_{BW}=0
- The primary instability is dominated by the P11 eigenmode & 2nd by the P10.
- The P11 evolves subcritically only.
- The P10 transcritically.
- Both subcritical branches exhibit limit points, which after further increase of the external pressure ε lead to energetically favorable branches. We proceed the solution until the two poles tend to coalesce.

Parametric study

- As we decrease the dimensionless bending modulus, the first instability is dominated by symmetric mode, for intermediate values by asymmetric and for very small again by symmetric (P24) mode.

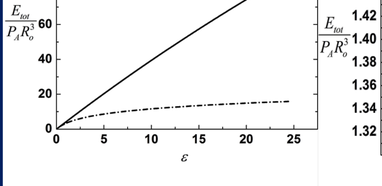

Fig.20 Bifurcation diagram

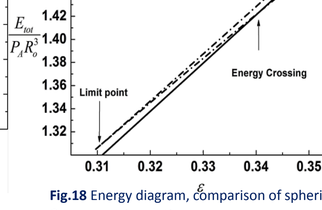

Fig.21 Bifurcation diagram

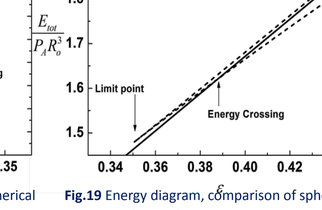

Fig.22 Bifurcation diagram

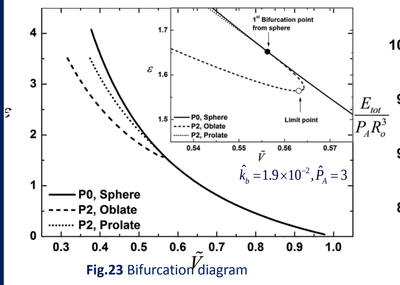

Fig.23 Bifurcation diagram

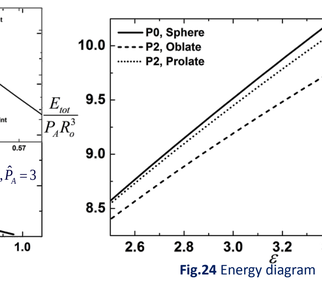

Fig.24 Energy diagram

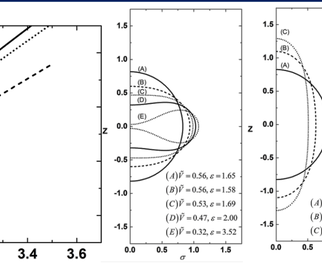

Fig.25 Oblate (right) & prolate (left) solutions

Simulation: MB covered with lipid

- k_b=3×10^{-14} Nm, χ=0.12 N/m
- R_o=3.6 μm, ν=0.5, Mooney-Rivlin, γ_{BW}=0.051 N/m
- The primary instability is dominated by the symmetric P2 mode and is evolved subcritically (Oblate & Prolate shapes)
- The oblate branch exhibits a limit, which changes very rapidly the response towards higher values of the pressure ε.

Parametric study

- As we increase the area dilatation modulus or decrease the dimensionless bending modulus the first instability is dominated by symmetric, then by asymmetric and finally by symmetric shapes.
- The above exchange of the primary stability shape is attributed to the effort of the shell to minimize its total energy.
- For relatively small area dilatation (χ) the shell minimizes its total energy with two indentations (symmetric shapes), but as χ increases the compressive stresses should be relaxed in favor of energetically favorable bending, thus a single indentation is formed (asymmetric shapes). However, further increase of χ requires two dimple to achieve static equilibrium. The above trend is detected in both types of shell via parametric study in dimensionless bending stiffness.

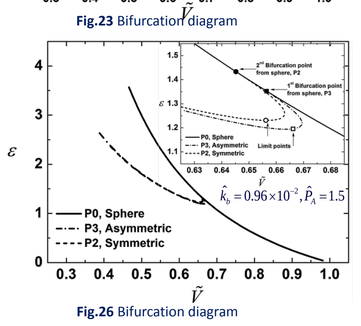

Fig.26 Bifurcation diagram

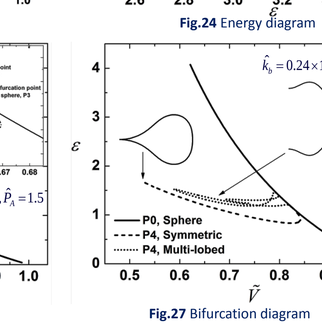

Fig.27 Bifurcation diagram

Discussion & Conclusions

- A theoretical model is presented for the static response of coated MB under the AFM and takes into account the thin liquid film between the cantilever and the shell due to hydrophilic nature of the shells.
- The total force is attractive or repulsive, when the height of the liquid film is higher or lower than the characteristic length δ_A.
- When the dimensionless pressure is relatively small, e.g. MB covered with polymer with big area dilatation modulus. The response in terms of force-deformation diagram is initially linear (~Δ) with flat shapes around the contact area and after the buckling point the response becomes non-linear (~$\Delta^{0.5}$).
- However, it is possible to bypass the buckling regime even if the bending is relatively small. This is the case where the gas pressure is equally important on the equilibrium and defines a new regime (~Δ^3). This behavior corresponds to MB covered with phospholipid monolayer, which usually have small area dilatation modulus.
- The last regime is also detected in the buckling curves for relatively high deformations.
- Parametric analysis shows that the dimensionless bending modulus controls the position of the buckling point.

- The elastic properties of microbubbles covered with thin polymeric shells can be estimated from AFM[6] measurements by the transition from the flat (Reissner) to the buckled (Pogorelov) branch.
- The elastic properties, namely area dilatation and bending modulus, of phospholipid shells can also be estimated from AFM[9] measurements by the transition from the bending stiffness (Reissner) regime to gas compressibility dominated regime.

- The intermolecular forces model is a novel theoretical tool that recovers the experimental f-d curves for microbubbles covered with either polymeric or phospholipid monolayer shells.

- Performing eigenvalue analysis for each case, we found that the spherical solution branch before any bifurcation point is characterized by one unstable eigenvalue, which is related with the imposition of the mass center at the origin of the axis in order to avoid translation as a rigid body.
- In both polymers and lipids, when the first bifurcation is dominated by an asymmetric mode, the secondary branch evolves subcritically and after a limit point evolves towards higher loads than the buckling threshold, where it tends to form a contact line in the region around the two poles.
- The second bifurcation is dominated by a symmetric mode which evolves transcritically. The subcritical branch evolves the same way as the asymmetric and is characterized by oblate shapes and the supercritical by prolate shapes.
- Both subcritical branches have more unstable eigenvalues in comparison with the sphere and higher energy, before exhibiting a limit point.
- However, after the limit point each of them loses one unstable eigenvalue in comparison with the branch that emerges right after the bifurcation point.
- The primary bifurcating branch, after the limit point, is linearly stable and additionally has lower energy as it evolves towards pole coalescence.
- Finally, there is a global stability behavior determined by minimum total energy. Below the bifurcation point and before the limit point, the energetically favorable configuration is a compressed sphere, but after the limit point the solutions with the lower energy are buckled which tend to coalesce.
- The above picture is corroborated when they are combined with numerical results from the dynamic buckling[13], where for loads higher than the buckling point buckled shapes characterize the solution, while below the bifurcation point spherical shapes are captured.

Selected References

1. Timoshenko S. & Woinowsky-Krieger, *Theory of plates & shells*. 1959: Mc-Graw-Hill.
2. Lytra, A., *Numerical & theoretical study of the static response of coated microbubbles subject to uniform and distributed load-Application on the estimation of the shell elastic properties*, PhD Thesis. University of Thessaly, 2017.
3. Blount, M.J., M.J. Miksis, and S.H. Davis, *The equilibria of vesicles adhered to substrates by short-ranged potentials.* Proc. R Soc. A, 2013. **469**(2153).
4. Updike, D.P. and A. Kalnins, *Axisymmetric Postbuckling and Nonsymmetric Buckling of a Spherical Shell Compressed Between Rigid Plates.* J. Appl. Mech. T ASME, 1972. **39**(1): p. 172-178.
5. Landau, L.D., et al., *Theory of Elasticity*. 1986: Butterworth-Heinemann.
6. Glynos, E., et al., *Nanomechanics of Biocompatible Hollow Thin-Shell Polymer Microspheres.* Langmuir, 2009. **25**(13): p. 7514-7522.
7. Lytra, A., N. Pelekasis, V. Sboros, E. Glynos, V. Koutsos, *Static Response of Coated Microbubbles: Modeling Simulations and Parameter Estimation*. Procedia IUTAM, 2015. **16**: p. 123-133.
8. Lulevich, V.V., D. Andrienko, and O.I. Vinogradova, *Elasticity of polyelectrolyte mutilayer microcapsules.* J. Chem. Phys., 2004. 120(8): p. 3822-3826.
9. Buchner Santos, E., et al., *Nanomechanical Properties of Phospholipid Microbubbles*. Langmuir, 2012. **28**(13): p. 5753-5760.
10. Lytra, A. & N. Pelekasis, *Static response and stability of coated microbubbles—multiplicity of solutions and parameter estimation*. Fluid Dyn. Res., 2014. **46**(4): p. 041422.
11. Barthes-Biesel, D., A. Diaz, and E. Dhenin, *Effect of constitutive laws for two-dimensional membranes on flow-induced capsule deformation*. JFM, 2002. **460**: p. 211-222.
12. Knoche, S. and J. Kierfeld, *Buckling of spherical capsules*. Physical Review E, 2011. **84**(4): p. 046608.
13. Vlachomitrou, M. & N. Pelekasis, *Dynamic simulation of a coated microbubble in an unbounded flow: Response to a step change in pressure*. JFM, 2017. **822**: p. 717-761.

Acknowledgments

This work was performed in the framework of the operational program: «Education and lifelong learning» - «**Aristeia I**» and was cofounded by the European Union (European Social Fund), national resources and the Department of Mechanical Engineering. The authors wish also to thank Dr. V. Koutsos, Dr. V. Sboros and Dr. E. Glynos for fruitful discussions on the AFM and for kindly providing the experimental (AFM) data.

European Union
European Social Fund
OPERATIONAL PROGRAMME EDUCATION AND LIFELONG LEARNING
Investing in knowledge society
MINISTRY OF EDUCATION & RELIGIOUS AFFAIRS
MANAGING AUTHORITY
NSRF 2007-2013
EUROPEAN SOCIAL FUND
Co-financed by Greece and the European Union